Terrestrial testbed for remote Coulomb spacecraft rotation control

Daan Stevenson* and Hanspeter Schaub

University of Colorado,
431 UCB, Boulder, CO 80309, USA
E-mail: daan.stevenson@colorado.edu
E-mail: hanspeter.schaub@colorado.edu
*Corresponding author

Abstract: A terrestrial testbed designed to investigate the torques between non-symmetric charged bodies is introduced. In practice, these torques may be used by spacecraft for touchless remote attitude control. The experimental system consists of a charged cylinder that rotates about its minor axis on a low friction bearing, while the electric potential on a nearby sphere is actively controlled to increase or decrease the rotation rate of the cylinder. A numerical simulation of the system that uses a previously developed reduced order electrostatic model is found to match the experimental data extremely well. Time dependent charge drain and disturbance torques on the cylinder are characterised so that they may be accurately modelled in the simulation. At low speeds, the achievable Coulomb torques are several times higher than the atmospheric drag and bearing friction. An active charge control de-spin manoeuvre arrests the cylinder motion in about 1/3 of the time it takes the cylinder to come to rest due to the friction in the system alone. Several hardware components and methods are identified for improvement in future iterations of the testbed, but the current result constitutes a successful verification of the Coulomb spacecraft de-spin concept.

Keywords: spacecraft Coulomb charging; remote attitude control; rotational testbed.

Reference to this paper should be made as follows: Stevenson, D. and Schaub, H. (2014) 'Terrestrial testbed for remote Coulomb spacecraft rotation control', *Int. J. Space Science and Engineering*, Vol. 2, No. 1, pp.96–112.

Biographical notes: Daan Stevenson earned his Bachelor of Science in Mechanical Engineering with a minor in Physics from the University of California Berkeley in 2008. He holds a Master of Science in Aerospace Engineering Sciences from University of Colorado Boulder (2011), and is currently a PhD candidate in the same department. He is funded by the NASA Science & Technology Research Fellowship, and was also awarded the NSF Graduate Research Fellowship and the DoD National Defense Science and Engineering Graduate Fellowship.

Hanspeter Schaub received his BS, MS and PhD degrees in Aerospace Engineering from Texas A&M University in 1992, 1994 and 1998. He is currently a Professor at the Aerospace Engineering Sciences Department at the University of Colorado at Boulder, researching non-linear dynamics and control, spacecraft formation flying, charged astrodynamics, space debris mitigation, and attitude control. He has published over 195 conference and journal papers, holds three patents, and is the lead author of a popular text book on spacecraft dynamics and control.

This paper is a revised and expanded version of a paper entitled 'Rotational testbed for coulomb induced spacecraft attitude control' presented at 5th International Conference on Spacecraft Formation Flying Missions and Technologies (SFFMT), Munich, Germany, 29–31 May 2013.

1 Introduction

Incidental electric charging is inherent in any spacecraft mission due to the interaction with the plasma environment both in Earth orbit and interplanetary space. NASA's ATS-5 and ATS-6 missions in 1969 and 1974 tested measurement capability of the spacecraft electrostatic potential and observed ambient charging up to –10 kV in solar eclipse (Olsen, 1985). Active voltage control with ion or electron emission devices, as tested in space on the 1979 SCATHA mission, (Mullen et al., 1986) is possible up to ± 10s of kV within milliseconds and at sub-milliwatt power levels (King et al., 2002). Generally, charge control devices are installed on satellites to mitigate natural charging and prevent electric anomalies, but a recent research effort has identified the feasibility of using Coulomb charge control to affect the relative motion of satellites flying in close proximity (King et al., 2002; Schaub et al., 2004). The use of electrostatic actuation is attractive for formation flying over conventional thrusters because non-renewable fuel reserves are not depleted and plume impingement issues are avoided. Moreover, if a spacecraft can impart relative potentials on itself and an inactive craft using a focused charged beam, touchless electrostatic manoeuvres may be achieved within non-cooperative formations (Schaub and Sternovský, 2013). One limitation of this technology is the effect of plasma in the low earth orbit (LEO) regime, which causes considerable Debye shielding of the electrostatic fields. Spacecraft formations at the sparser geosynchronous (GEO) space environment, however, can exert milliNewton level electrostatic forces at separation distances of tens of metres using tens of kilovolts of potential (King et al., 2002). Debye lengths in the GEO regime tend to be 180 metres or higher, and even during denser and colder plasma conditions, the large potentials considered for this concept result in effective Debye lengths much larger than the intended separation distances (Stiles et al., 2012).

Investigation of the charged Coulomb interaction between non-spherical bodies suggests that prolate bodies can experience torques and off-axis forces (Jasper and Schaub, 2011). If these torques can be harnessed to remotely decrease the rotation of non-cooperative bodies with large moments of inertia and angular momenta, the tradespace of candidate spacecraft for rendezvous and docking operations can be greatly increased. Pose algorithms and attitude matching manoeuvres for rendezvous are generally limited to rotation rates below 1 deg/s (Rembala et al., 2012). However, implementation of the remote Coulomb de-spin concept depicted in Figure 1 could reduce ambient rotation rates prior to docking operations. This technology is applicable to various mission scenarios intended to ameliorate the expanding orbital debris situation at GEO (Anderson and Schaub, 2013). First, while an electrostatic tug can be used to increase the semi-major axis of a GEO debris object by 300 km in two months (Schaub and Moorer, 2010; Hogan and Schaub, 2011), a docked Hohmann transfer would accomplish this in just over 12 hours. By remotely reducing the rotation rate prior to

rendezvous, collision risks and guidance and control challenges are greatly reduced during docking operations. An alternative to repositioning derelict satellites into a graveyard orbit is to service them by replenishing fuel reserves or repairing failed components. Such missions, as investigated by NASA's Satellite Servicing Capability Office and DARPA's Phoenix program, preclude the unnecessary insertion of replacement satellites.

Figure 1 Depiction of the remote Coulomb de-spin concept (see online version for colours)

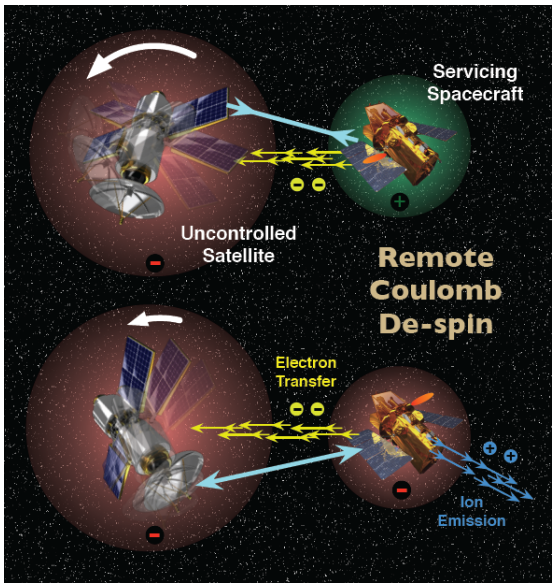

In order to accurately predict the relative motion dynamics of Coulomb spacecraft formations and develop appropriate charge control strategies, the electrostatic interactions must be modelled with high fidelity. Figure 2 compares the accuracy and computational cost of various electrostatic models. During previous research efforts, charged spacecraft are modelled by point charges (Wang, 2010) or by conducting spheres (Seubert and Schaub, 2010). Because they lack the ability to resolve the charge distribution in non-symmetric bodies, these methods are incapable of predicting electrostatic torques and off-axis forces. The finite element analysis (FEA) approach at the other end of the spectrum yields highly accurate numerical solutions, but lacks the computational speed necessary for 6 degree of freedom (6DOF) charged relative motion simulations. The recently developed multi-sphere method (MSM) uses a set of conductive spheres throughout the geometry of a spacecraft to capture the 3D electrostatic effects, thus achieving the desired balance between computational efficiency and accuracy. A reduced number of spheres can be distributed within the volume of simpler geometries, (Stevenson and Schaub, 2012a) or a larger number can be used to uniformly populate the surface of more complex shapes (Stevenson and Schaub, 2012b). The MSM is utilised to investigate the Lyapunov stability and simulate implementation of the non-linear control algorithms necessary for the remote de-spin of a rotating cylinder by active Coulomb charging (Schaub and Stevenson, 2012). It is desirable to further verify this concept experimentally, and this paper outlines the terrestrial testbed that has been developed to do so.

Figure 2 Comparison of various electrostatic models (see online version for colours)

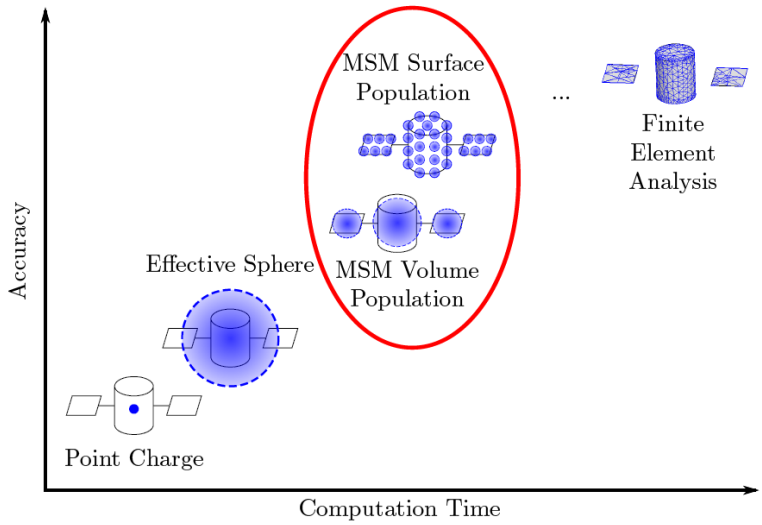

2 Multi-sphere method

The multi-sphere model (MSM) framework is presented here as applied to the cylinder-sphere system shown in Figure 3 (Schaub and Stevenson, 2012). The cylinder shape is representative of many upper stage rocket bodies such as the Centaur, which may experience a tumbling motion that must be removed if any spacecraft wishes to perform a docking manoeuvre. While it is possible to capture the induced charge effects that occur at very close proximity scenarios with a larger set of spheres distributed on the surface of the objects (Stevenson and Schaub, 2012b), three spheres are sufficient to capture the torques exerted on the cylinder at larger separations distances.

Figure 3 Three-sphere MSM for cylinder-sphere configuration (see online version for colours)

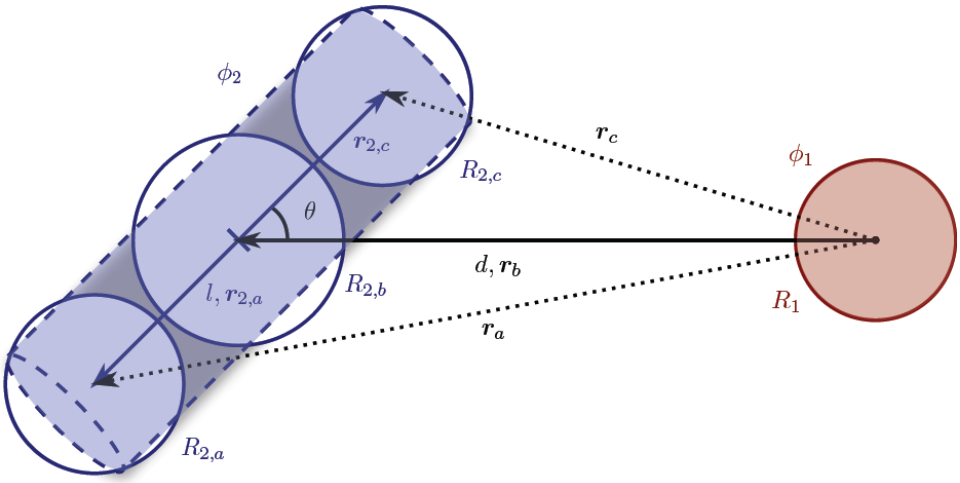

The defining system parameters are the separation distance d, the cylinder orientation angle θ, and the control voltages ϕ_1 and ϕ_2. The spheres in the cylinder are separated by l while the remaining relative distances are:

$$r_a = \sqrt{l^2 + d^2 + 2ld\cos\theta} \tag{1}$$

$$r_b = d \tag{2}$$

$$r_c = \sqrt{l^2 + d^2 - 2ld\cos\theta} \tag{3}$$

The electrostatic forces are determined by the charges residing on each sphere. These result from the prescribed electric potentials, according to the self and mutual capacitance relationships in equation (4), where k_c = 8.99 × 10^9 Nm^2/C^2 is Coulomb's constant (Smythe, 1968; Sliško and Brito-Orta, 1998; Seubert and Schaub, 2010):

$$\phi_i = k_c \frac{q_i}{R_i} + \sum_{j=1, j\neq i}^{m} k_c \frac{q_j}{r_{i,j}} \tag{4}$$

These relations can be combined for each sphere to obtain the matrix equation

$$\begin{bmatrix} \phi_1 \\ \phi_2 \\ \phi_3 \\ \phi_4 \end{bmatrix} = \underbrace{k_c \begin{bmatrix} 1/R_1 & 1/r_a & 1/r_b & 1/r_c \\ 1/r_a & 1/R_{2,a} & 1/l & 1/2l \\ 1/r_b & 1/l & 1/R_{2,b} & 1/l \\ 1/r_c & 1/2l & 1/l & 1/R_{2,c} \end{bmatrix}}_{[C_M]^{-1}} \begin{bmatrix} q_1 \\ q_a \\ q_b \\ q_c \end{bmatrix} \tag{5}$$

By inverting $[C_M]^{-1}$, the charge on each sphere is determined at any instant of time. The total electrostatic force $\boldsymbol{F}_2$ and torque $\boldsymbol{M}_2$ about the centre of the cylinder are then given by the summations

$$\boldsymbol{F}_2 = k_c q_1 \sum_{i=a}^{c} \frac{q_i}{r_i^3} \boldsymbol{r}_i \tag{6}$$

$$\boldsymbol{M}_2 = k_c q_1 \sum_{i=a}^{c} \frac{q_i}{r_i^3} \boldsymbol{r}_{2,i} \times \boldsymbol{r}_i \tag{7}$$

For a body with inertia matrix $[I]$ and angular velocity vector ω rotating freely in space, the rotational equations of motion are

$$[I]\dot{\omega} = -\omega \times [I]\omega + \boldsymbol{M} \tag{8}$$

The control and dynamics of a Coulomb actuated spacecraft with three degrees of rotation is beyond the scope of this study, but will be investigated at a later time. For now, we constrain the cylinder with transverse moment of inertia I_{cyl} to one dimensional motion in the plane of the control sphere, as is the case for the experimental setup. The dynamics then reduce to

$$I_{cyl}\ddot{\theta} = M_2 \tag{9}$$

where equation (7) can be simplified as follows:

$$M_2 = k_c q_1(d,\theta) l d \sin\theta \left(\frac{q_c(d,\theta)}{r_c^3(d,\theta)} - \frac{q_a(d,\theta)}{r_a^3(d,\theta)} \right) \tag{10}$$

Meanwhile, there is a net attractive or repulsive force acting between the two objects in the system. In space, the control craft (the sphere) must create a thrusting force to oppose this Coulomb interaction, thus providing the external influence needed to remove the cylinder's angular momentum from the system. In the terrestrial experiment, the sphere mount and cylinder bearing provide the constraints necessary to oppose these Coulomb forces.

3 Experimental setup

All hardware components of the terrestrial testbed for electrostatic attitude control are shown in Figure 4. The cylinder, constructed with a conducting surface, has a 15 cm diameter and a 45 cm length. The mass of the rotating components is 182.1 g, with a transverse moment of inertia of 3.30 g·m^2. The 15 cm diameter stationary sphere has a 15 cm surface to surface separation from the cylinder at a parallel orientation with $\theta = 0°$. Table 1 gives the dimensions as outlined in Figure 3, where the MSM parameters are scaled down from the optimised set found by Stevenson and Schaub (2012a).

Figure 4 Components of the terrestrial testbed for electrostatic attitude control (see online version for colours)

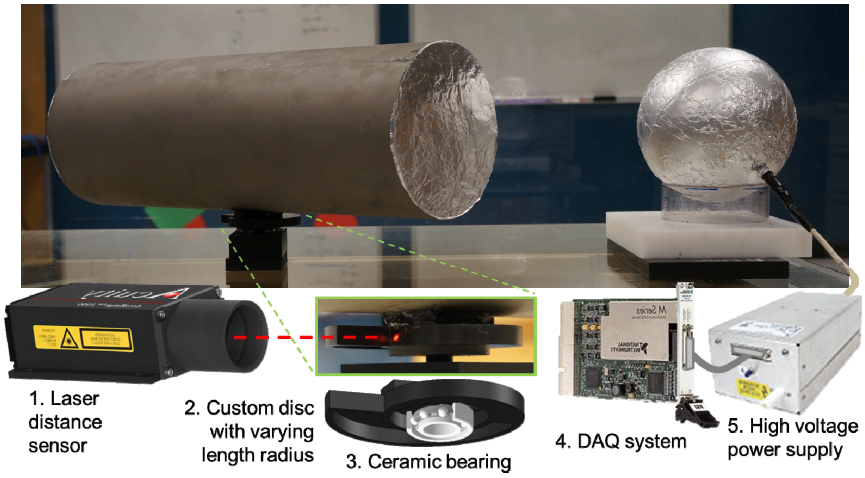

The three critical components for the rotational Coulomb testbed are low friction rotation, angular position feedback, and high voltage electrostatic control. Several options were considered to achieve frictionless rotation for the cylinder. Ultimately, a full ceramic miniature ball bearing was implemented. Friction disturbance torques are minimal, as characterised in the next section, and the material functions as a successful insulator between the charged cylinder and the base on which the bearing is mounted.

Table 1 Parameters for cylinder attitude control system

Parameter	*Value*	*Units*	*Description*
m_{Cyl}	182.1	g	Cylinder mass
I_{cyl}	3.30	g·m^2	Cylinder transverse moment of inertia
d	45	cm	Object centre-to-centre separation
l	17.353	cm	MSM parameters
R_a, R_c	8.8634	cm	MSM parameters
R_b	9.7664	cm	MSM parameters

To apply the desired Coulomb attitude control algorithms, knowledge of the rotational position of the cylinder is necessary. The USB-input laser distance sensor from the heritage linear Coulomb testbed is currently utilised to make this measurement. It is focused on the varying radius edge of the custom CNC machined plastic part in Figure 5, which rotates along with the cylinder. The radius is equal to $r = 1 + \xi / 2\pi$ inches so that an absolute angle can be deduced from the linear measurement. The bottom is recessed in such a way that the inertial axis remains aligned with the axis of rotation on the bearing. The laser is capable of a 50 Hz sampling frequency, but because it is intended for longer range measurement, the output is inherently noisy on the one inch variation surface. A roughly 2 Hz error oscillation with a 1σ standard deviation of 2 deg is identified. When differentiated to determine the speed and acceleration of the rotating cylinder, the noise can lead to severe uncertainties in the results. As such, a first order low pass filter is applied at each differentiation step, with a cut-off frequency $\omega_v = 1$ Hz for the angular velocity and $\omega_v = 0.1$ Hz for the angular acceleration. A similar in-situ filter is applied when determining the angular velocity for the Coulomb control algorithms.

Figure 5 Custom linear-rotational measurement conversion part (see online version for colours)

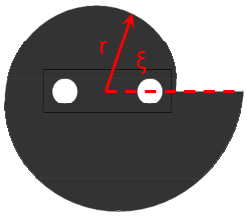

For the voltage control of the external sphere and the initial charging of the cylinder, two Spellman CZE 2000 high voltage power supplies are used. They are capable of supplying ± 30 kV at up to 300 μA, which results in power levels well within typical safety limits when proper precaution measures are practiced. One limitation of the power supplies is that they exhibit a slight reduction in output magnitude and a time delay as large as 1 second when switching polarities (Seubert, 2011). For the simulations presented in this paper, the lag is modelled as a constant 0.8 second delay whenever the voltage switches from zero to a non-zero quantity. The power supplies are controlled by a PCI express based 16-bit multi-channel NI DAQ card. The entire system is monitored and directed by a custom GUI developed with Mac OS-X's native objective C architecture Cocoa. The following list identifies the manufacturer and model numbers for all the hardware mentioned above.

1 laser distance sensor: 'Acuity Laser Measurement AccuRange AR1000'

2 custom disc with varying length radius – machined in-house

3 ceramic bearing: '608-2RS 8 × 22 × 7 full ceramic sealed bearing'

4 DAQ system: 'National Instruments PXI-6259 data acquisition card and (2X) NI SCB-68 shielded breakout boxes'

5 high voltage power supply: 'Spellman Voltage Electronics Corporation CZE 2000'.

3.1 Modelling disturbances

Besides the Coulomb interaction with the sphere, the clearly identifiable disturbances acting on the cylinder as it rotates about its axis are the friction torque from the bearing and the atmospheric drag force acting on the cylinder surface.

The friction torque M_B in a rolling bearing is due to a combination of radial forces and axial forces F_i, the friction coefficient μ_i and the average of the bore and outside diameter of the bearing $\bar{d} = \frac{d_i + d_o}{2}$, as follows:

$$M_B = \mu_r \frac{\bar{d}}{2} F_r + \mu_a \frac{\bar{d}}{2} F_a \tag{11}$$

Since the expected radial force due to the Coulomb interaction with the sphere never exceeds 13.90 mN, whereas the weight of the cylinder and laser disc is equal to a 1.786 N axial force, the radial component can be neglected. If the bearing diameter is incorporated into a new combined bearing friction coefficient γ, the total bearing friction is written

$$M_B = \gamma F_a \tag{12}$$

where γ will be determined empirically, because there is no readily available way to isolate the bearing friction torque from other disturbance torques such as atmospheric drag.

For high Reynolds number flows, the drag force F_D on a body with surface area A and drag coefficient C_d moving at velocity V through a medium with density ρ is given by

$$F_D = \frac{1}{2} \rho V^2 C_d A \tag{13}$$

Consider a cylinder with length L and diameter D rotating at angular rate ω. A differential slice of width dr located at a distance r away from the cylinder axis of rotation experiences a drag force

$$\mathrm{d}F_D = \frac{1}{2} \rho (\omega r)^2 C_d (D \mathrm{d}r) \tag{14}$$

The differential torque from each slice is $dM = rdF$ and the total torque from both halves of the cylinder due to atmospheric drag is

$$M_D = \rho \omega^2 C_d D \int_0^{L/2} r^3 \mathrm{d}r \tag{15}$$

$$M_D = \frac{\rho\omega^2 C_d D L^4}{64} \tag{16}$$

A typical atmospheric air density ρ = 1.194 kg/m^3 is used and C_D is found to be 1 for an infinite cylinder at mid-range Reynold numbers (Tritton, 1988). The parasitic drag across the two ends of the cylinder must be considered. Since the ends move at $V = \omega \frac{L}{2}$ relative to the ambient air, this effect can be incorporated in the empirically determined C_d value.

3.2 *Empirical determination of disturbance parameters*

Both modelled disturbance phenomena contain an unknown coefficient that must be determined empirically. Five sets of data are collected by giving the cylinder an initial rotation and allowing it to de-spin naturally while the electric potential on both the cylinder and the adjacent sphere are held at zero. Figure 6(a) shows the angular rates of the cylinder for each experimental run and a simulated de-spin using the modelled disturbance torques from equations (12) and (16). The corresponding coefficients were tuned until the resultant angular velocity curve fit the experimental data well, resulting in γ = 0.00003 and C_d = 1.05. Figure 6(b) shows the resulting disturbance torques in the simulation, suggesting that the drag force is dominant at angular rates higher than 38 deg/s.

Figure 6 Characterisation of disturbance torques, (a) angular velocity, simulated and experimental (b) disturbance torques, simulated (see online version for colours)

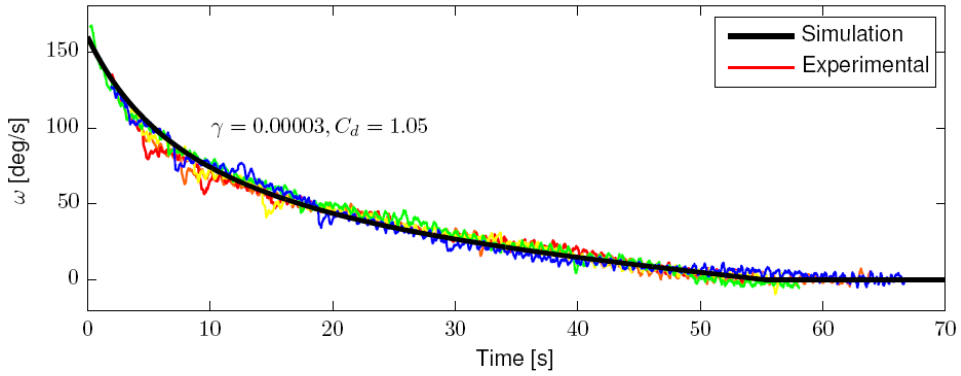

(a)

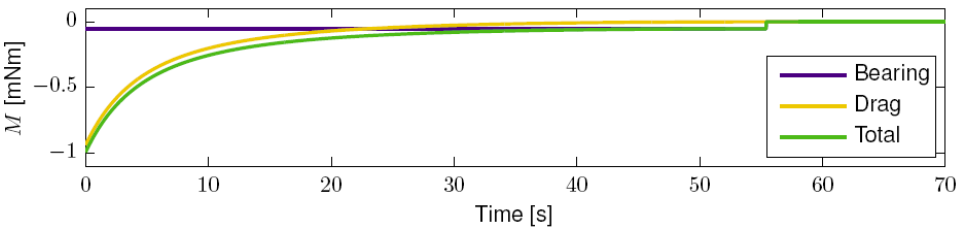

(b)

4 Passive charging

Active charging of a spinning cylinder is difficult to implement while minimising disturbance torques at the bearing about which the cylinder rotates. Therefore, in this iteration of the testbed, passive charging is employed. While the electric potential on the sphere is actively controlled throughout the experiment, the cylinder is brought to a desired voltage initially, after which the charging lead is removed and the cylinder is left with a floating charge. In order to accurately model this scenario, modifications must be made to the MSM to account for a body that carries a specific charge instead of maintaining a prescribed voltage. Moreover, the natural charge drain due to interaction with the atmospheric environment and the insulated bearing module must be characterised.

4.1 MSM modification

Assuming no charge bleeding for now, the scenario presented above entails that the cylinder maintains a total charge

$$q_2 = q_a + q_b + q_c \tag{17}$$

determined by the configuration at which the charge lead is removed. From this point on, ϕ_2 is an unknown dependent on ϕ_1 and the relative position and orientation of the two conductors, but there is also an extra linear equation in equation (17). In order to isolate all the unknowns in equation (5) into a single column vector, the matrix equation must be modified as follows:

$$\begin{bmatrix} \phi_1 / k_c \\ 0 \\ 0 \\ 0 \\ q_2 \end{bmatrix} = \begin{bmatrix} 1/R_1 & 1/r_a & 1/r_b & 1/r_c & 0 \\ 1/r_a & 1/R_{2,a} & 1/l & 1/2l & -1 \\ 1/r_b & 1/l & 1/R_{2,b} & 1/l & -1 \\ 1/r_c & 1/2l & 1/l & 1/R_{2,c} & -1 \\ 0 & 1 & 1 & 1 & 0 \end{bmatrix} \begin{bmatrix} q_1 \\ q_a \\ q_b \\ q_c \\ \phi_2 / k_c \end{bmatrix} \tag{18}$$

It is necessary to incorporate the factor k_c with the electric potential terms prior to this modification to ensure that the matrix that must be inverted remains well-conditioned. This approach can be extended for any system where a conductor contains a floating charge rather than being held at a specific voltage.

4.2 Surface voltmeter measurements

Measuring the electrostatic potential on a conducting body with a floating charge is not achievable with conventional high voltage measurement equipment. Using the MSM, which is shown to accurately predict the capacitance of a modelled geometry (Stevenson and Schaub, 2012b), the capacitance of the 45 cm by 15 cm cylinder is 1.6407×10^{-11} F. Even if a contact voltmeter with 1 GΩ impedance is used, the time constant $\tau = RC$ of the measurement circuit is a small fraction of a second, thus preventing accurate measurements. Instead, an AlphaLab Inc. Model SVM2 DC Surface Voltmeter as shown in Figure 7 is used to quantify the voltage and charge present on the floating cylinder. The metal disc on the rear of the voltmeter is connected to a high impedance amplifier.

When the disc is in the presence of an electric field, charged particles are drawn from the circuit to the surface of the disc, which is measured by the amplifier. The meter is calibrated so that when the disc is held a prescribed distance from a conducting surface, the voltage on the object can be deduced. The measurement range is specified to ± 30 kV, but in reality the meter saturates at roughly –16 kV and only + 6 kV due to the presence of positive ions.

Figure 7 AlphaLab Inc. Surface DC Voltmeter, Model SVM2 (see online version for colours)

The SVM2 surface voltmeter was used to measure the remaining voltage on the cylinder for 120 seconds after it was charged to $V = -15$ kV and the charging lead was removed and controlled to 0 V. The orientation of the cylinder was held at both $\theta = 0°$ (parallel) and $\theta = 90°$ (perpendicular) orientations, while the voltage on the nearby sphere was varied between ± 15 kV. The results are plotted in Figure 8(a), from which it is clear that the perpendicular orientation drains charge faster than the parallel orientation, while the opposite sphere polarity case drains voltage faster than the same polarity one. For each scenario, measurements were taken along the minor axis of the cylinder as well as the major axis, but the variation was minor and no trends were discernible between the two, as expected because the conducting cylinder represents an equipotential surface. Figure 8(b) shows an extended time measurement of the median case. As the trend suggests an initial exponential drop followed by a linear decline in voltage, the function

$$V(t) = V_0\left[0.87 - 0.00041t - 0.127e^{-0.017t}\right] \tag{19}$$

is fit to the curve, with $R^2 = 0.9996$. A charge drain with these parameters is implemented in the active charge control simulations designed to match the experimental results.

It is important to remember that once the voltage lead has been removed and the charge has been delivered to the cylinder, changes in the orientation of the cylinder or the voltage level of the sphere will affect the electrostatic potential of the cylinder but not the total charge residing on its surface. To minimise the variation then, the charge should be deposited on the cylinder while the sphere is held grounded ($\phi_1 = 0$ V). The voltage measured on the cylinder by the surface voltmeter as the sphere potential switches

polarity agrees with expected levels from the MSM, and switching does not affect the rate of charge drain. Moreover, voltage drain rates were measured at both smaller and positive initial voltages, and the remaining voltage scales linearly with initial voltage, which allows for extrapolation to higher voltages. The total charge on the cylinder is also found to scale linearly with its voltage for a given orientation and sphere potential. Therefore, the sum of the charges q_2 sees a time-dependent reduction by $q_2(t) = q2{,}0[0.87 - 0.00041t + 0.127e^{-0.017t}]$, which is the formulation used in the following simulations.

Figure 8 Characterisation of charge drain on floating cylinder (a) charge drain, various configurations (b) charge drain, curve fit (see online version for colours)

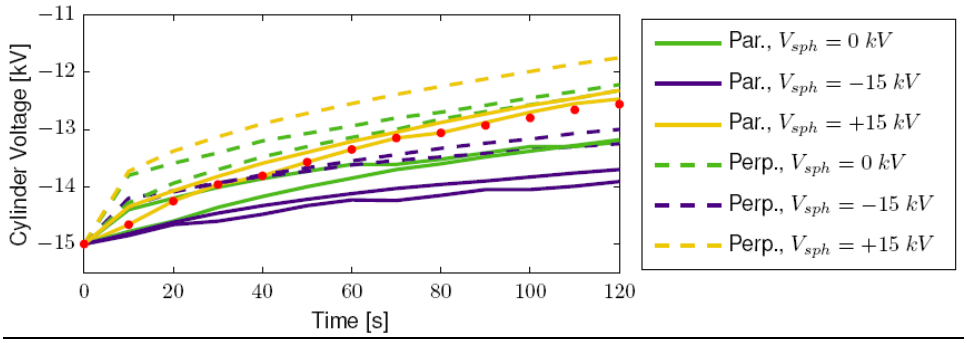

(a)

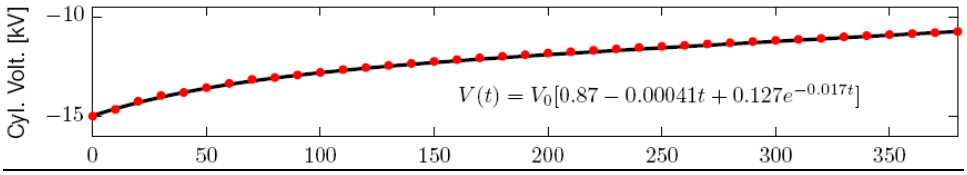

(b)

5 Active charging results

With the disturbance torques and passive charge drain on the cylinder fully characterised, various simple charge control experiments are executed. The results are rigorously compared to an inclusive numerical simulation of the same system. MATLAB's 'ode45' function is used for the integration, while the three-sphere MSM is implemented to predict the Coulomb torques present on the rotating cylinder. First, active spin-up control is analysed to determine at what angular velocity the drag and friction torques will balance the Coulomb torques from active charge control on the external sphere. Next, a de-spin control algorithm is implemented and compared to the natural velocity reduction resulting from bearing friction and atmospheric drag alone.

5.1 Spin-up control

The voltage control algorithm outlined in Table 2 is applied to the sphere so that a constant rotation rate is maintained on the cylinder. When the angle falls within the dead band value θ_{DB} = 5 deg of the perpendicular and parallel cylinder configurations, zero potential is applied to the sphere. This ensures that uncertainties in the knowledge of the cylinder angle do not result in undesired torques on the cylinder. The simulation starts with a cylinder rate of ω_0 = 60 deg/s. Figure 9 displays various aspects of the experimental and simulated operation. As seen by the cylinder angular velocity in Figure 9(a), there is a very impressive level of agreement between the experimental and simulated results. While the oscillations in the experimental signal are likely due to measurement noise, the simulated rotation rate also shows some periodicity due to the complex Coulomb interactions. There even appears to be a slight oscillation in magnitude with a period of about 40 seconds that is evident in both curves, although there is no clear justification for this trend in the numerical simulation.

Table 2 Voltage control law for spin-up procedure

	$0° + \theta_{DB} < \theta < 90° - \theta_{DB}$ $180° + \theta_{DB} < \theta < 270° - \theta_{DB}$	$90° + \theta_{DB} < \theta < 180° - \theta_{DB}$ $270° + \theta_{DB} < \theta < 360° - \theta_{DB}$
CCW ($\omega > 0$)	$\phi_1 = -30$ kV	$\phi_1 = +30$ kV
CCW ($\omega < 0$)	$\phi_1 = +30$ kV	$\phi_1 = -30$ kV

The voltage signals in Figure 9(b) exhibit the effect of the 0.8 second lag in the power supply as it switches polarity. When this lag is removed from the simulation, rotation rates up to 90 deg/s can be maintained. The voltage ϕ_2 on the cylinder varies slightly along with the switching polarity of the sphere voltage. Its slowly decreasing trend due to the charge drain is also visible. Figure 9(c) shows that the Coulomb torques achievable in this terrestrial system are about four times higher than the disturbances, which are dominated by atmospheric drag since the cylinder rotates above 50 deg/s. The Coulomb torques are not symmetric, because the induced charge effect causes much higher torques in the opposite polarity attraction scenario than for the same polarity repulsion case.

5.2 De-spin control

For the cylinder de-spin experiment, the exact opposite voltage control of Table 2 is applied to the sphere. Differentiation of the orientation signal is performed by the controller, using an in-situ version of the low-pass filter discussed in Section 3. A velocity dead band ω_{DB} = 4 deg/s is also applied to ensure that uncertainties in the differentiated velocity do not result in undesired torques as the cylinder comes to a halt. Figures 10(a) and 10(b) show the cylinder angle and rotation rate from both the physical experiment and the numerical simulation, with initial conditions θ_0 = 265 deg and ω_0 = 105 deg/s. The majority of the rotation is removed from the system within 18 seconds, which is far shorter than the 50 seconds it takes to arrest the same rotation rate without Coulomb control as in Figure 6(a). This constitutes a successful demonstration of the Coulomb de-spin concept in a terrestrial environment. Without the

delay in the power supply present, de-spin time is reduced to 14 seconds, which is a smaller difference than for the spin-up case. This is because the atmospheric drag torque is dominant at the higher rates, while the lag in the power supply is less severe for lower rates as the cylinder switches quadrants less rapidly. Plots of the applied voltages and moments are omitted for brevity.

Figure 9 Cylinder spin-up: experimental and simulation (a) angular velocity (b) simulated electric potentials (c) simulated torques (see online version for colours)

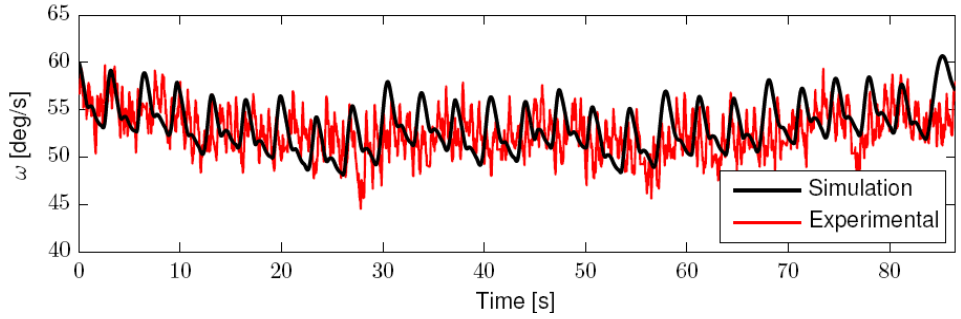

(a)

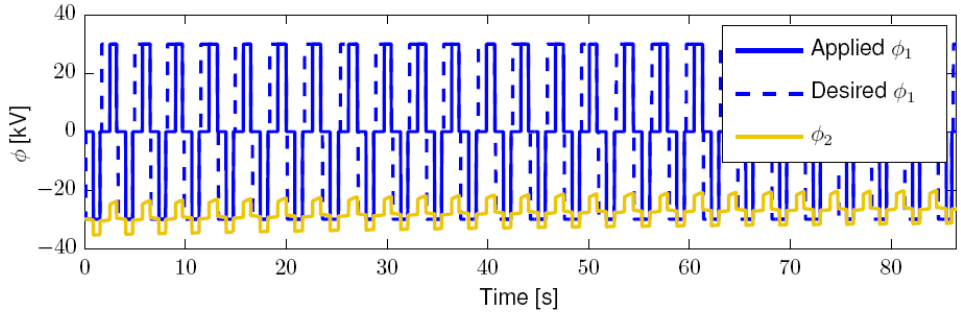

(b)

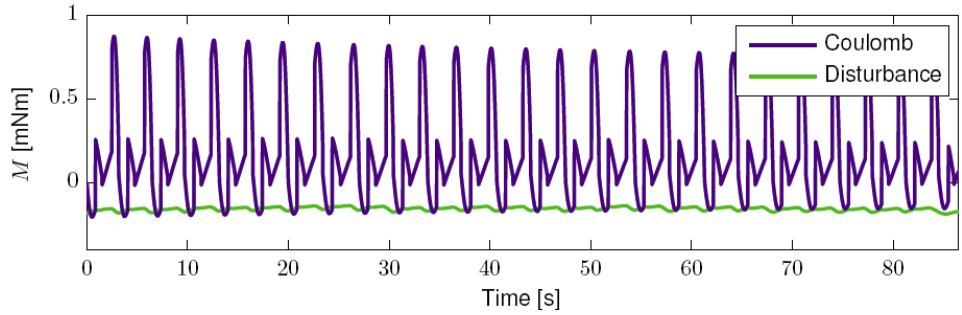

(c)

Figure 10 Cylinder de-spin: experimental and simulation, (a) rotation angle (b) angular velocity (see online version for colours)

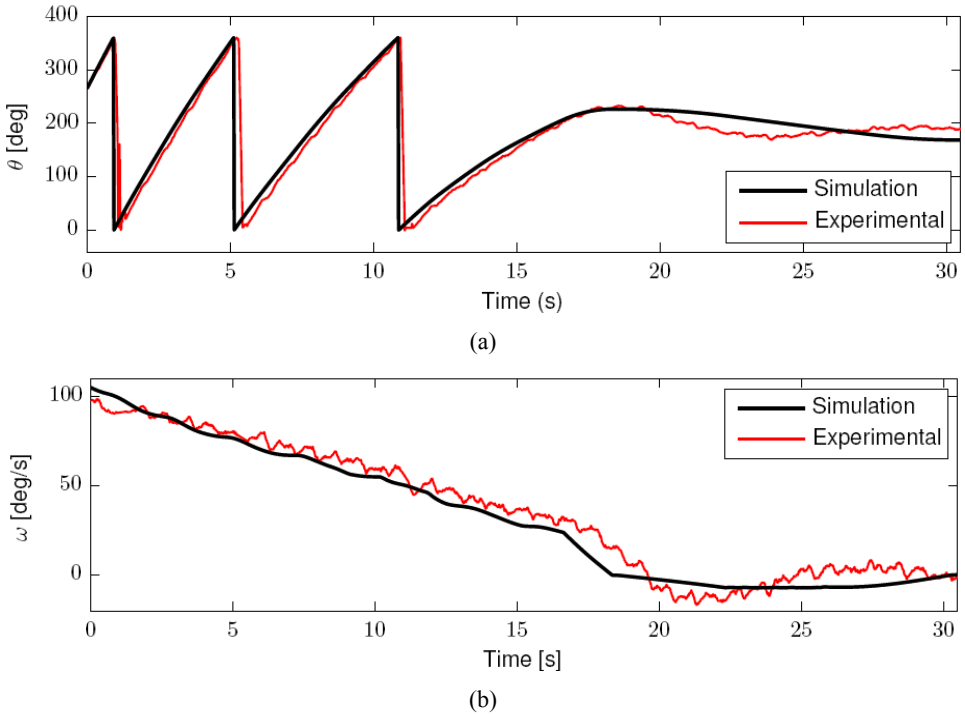

(a)

(b)

6 Conclusions

A terrestrial testbed has been created to verify the concept of remote attitude control by Coulomb charging. Various physical parameters in the system are characterised such as the charge drain from the floating potential cylinder and coefficients for the bearing friction and atmospheric drag. The disturbance torque from atmospheric drag is dominant at rotational speeds above 38 deg/s, below which the constant friction torque from the ceramic bearing dominates. Charge drain from the cylinder due to interaction with the atmosphere and its mount is minimal, as it retains 80% of its charge even after 3 minutes. Simulations using a multi-sphere model with three spheres match exceptionally well with the experimental data, for both a charge controlled spin-up procedure and an active charged de-spin. Coulomb torques up to four times larger than the notable disturbance torques are achieved, and the largest impedance to the Coulomb actuation is the delay present in the high voltage power supply when switching polarities. The noise and inaccuracies present in the current attitude encoding method are manageable for this application by signal processing, but in order to validate more precise attitude control algorithms, a more accurate means of encoding is desirable. In the end, this testbed represents successful experimental verification of terrestrial charged remote attitude control in one dimension. Mapping the testbed results to a realistic GEO mission scenario is a challenging future task. Expansion to higher dimensional control and more generic spacecraft shapes can be conducted by altering the controlled shape and its axis of

rotation. Moreover, future modification of the MSM will account for Debye shielding effects, as well as dielectric and non-conducting spacecraft materials.

Acknowledgements

This material is based upon work supported by the NASA Science and Technology Research Fellowship (NASA Grant #NNX11AN47H).

References

Anderson, P.V. and Schaub, H. (2013) 'Local debris congestion in the geosynchronous environment with population augmentation', *6th European Conference on Space Debris*, Darmstadt, Germany, 22–25 April 2013.

Hogan, E. and Schaub, H. (2011) 'Relative motion control for two-spacecraft electro-static orbit corrections', *AIAA Journal of Guidance, Control, and Dynamics*, Vol. 36, No. 1, pp.240–249.

Jasper, L.E.Z. and Schaub, H. (2011) 'Effective sphere modeling for electrostatic forces on a three-dimensional spacecraft shape', *AAS/AIAA Spaceflight Mechanics Meeting*, Girdwood, Alaska, 31 July–4 August.

King, L.B., Parker, G.G., Deshmukh, S. and Chong, J-H. (2002) 'Spacecraft formation-flying using inter-vehicle Coulomb forces', Technical report, NASA/NIAC.

Mullen, E.G., Gussenhoven, M.S., Hardy, D.A., Aggson, T.A., Ledley, B.G. and Whipple, E. (1986) 'Scatha survey of high-level spacecraft charging in sunlight', *Journal of Geophysical Research: Space Physics*, Vol. 91, No. A2, pp.1474–1490.

Olsen, R. (1985) 'Experiments in charge control at geosynchronous orbit – ats-5 and ats-6', *Journal of Spacecraft and Rockets*, Vol. 22, No. 3, pp.254–264.

Rembala, R., Teti, F. and Couzin, P. (2012) 'Operations concept for the robotic capture of large orbital debris', *35th Annual AAS Guidance & Control Conference*, Breckenridge, Colorado, 3–8 February.

Schaub, H. and Moorer, D.F. (2010) 'Geosynchronous large debris reorbiter: challenges and prospects', *AAS Kyle T. Alfriend Astrodynamics Symposium*, Monterey, California, 17–19 May.

Schaub, H. and Sternovský, Z. (2013) 'Active space debris charging for contactless electrostatic disposal maneuvers', *6th European Conference on Space Debris*, Darmstadt, Germany, 22–25 April.

Schaub, H. and Stevenson, D. (2012) 'Prospects of relative attitude control using coulomb actuation', *Jer-Nan Juang Astrodynamics Symposium*, College Station, Texas, 25–26 June.

Schaub, H., Parker, G.G. and King, L.B. (2004) 'Challenges and prospect of coulomb formations', *Journal of the Astronautical Sciences*, Vol. 52, Nos. 1–2, pp.169–193.

Seubert, C. (2011) *One-Dimensional Spacecraft Formation Flight Testbed for Terrestrial Charged Relative Motion Experiments*, Unpublished PhD thesis, University of Colorado, Boulder, Colorado.

Seubert, C.R. and Schaub, H. (2010), 'Electrostatic force model for terrestrial experiments on the coulomb testbed', *61st International Astronautical Congress*, Prague, Czech Republic, 27 September–1 October.

Sliško, J. and Brito-Orta, R.A. (1998) 'On approximate formulas for the electrostatic force between two conducting spheres', *American Journal of Physics*, Vol. 66, No. 4, pp.352–355.

Smythe, W.R. (1968) *Static and Dynamic Electricity*, 3rd ed., McGraw-Hill, New York.

Stevenson, D. and Schaub, H. (2012a) 'Multi-sphere method for modeling spacecraft electrostatic forces and torques', *Advances in Space Research*, Vol. 35, No. 3, pp.10–20.

Stevenson, D. and Schaub, H. (2012b) 'Optimization of sphere population for electrostatic multi sphere model', *12th Spacecraft Charging Technology Conference*, Kitakyushu, Japan, 14–18 May.

Stiles, L.A., Seubert, C.R. and Schaub, H. (2012) 'Effective coulomb force modelling in a space environment', *AAS Spaceflight Mechanics Meeting*, Charleston, South Carolina, 29 January–2 February.

Tritton, D. (1988) *Physical Fluid Dynamics*, Oxford Science Publications, Clarendon Press, Oxford.

Wang, S. (2010) *Shape Control of Charged Spacecraft Cluster with Two or Three Nodes*, Unpublished PhD thesis, University of Colorado, Boulder, Colorado.